Journal of Molecular Structure 1240 (2021) 130612

Contents lists available at ScienceDirect

Journal of Molecular Structure

journal homepage: www.elsevier.com/locate/molstr

Eudesmic acid-polyoxomolybdate organo-conjugate as novel anticancer agent

Maryam Ramezani-Aliakbari[a], Azim Soltanabadi[b], Hojjat Sadeghi-aliabadi[a], Jaleh Varshosaz[c], Bahram Yadollahi[d], Farshid Hassanzadeh[a], Mahboubeh Rostami[e,*]

[a] Department of Medicinal Chemistry, School of Pharmacy and Isfahan Pharmaceutical Sciences Research Center, Isfahan University of Medical Sciences, Isfahan, Iran
[b] Department of Physical Chemistry, Faculty of Chemistry, Razi University, P.O. Box: 6714967346, Kermanshah, Iran
[c] Novel Drug Delivery Systems Research Center and Department of Pharmaceutics, School of Pharmacy and, Isfahan University of Medical Sciences, Isfahan, Iran
[d] Department of Chemistry, University of Isfahan, Isfahan, Iran
[e] Novel Drug Delivery Systems Research Center and Department of Medicinal Chemistry, School of Pharmacy and Pharmaceutical Sciences and, Isfahan University of Medical Sciences, Isfahan, Iran

ARTICLE INFO

Article history:
Received 10 February 2021
Revised 28 April 2021
Accepted 29 April 2021
Available online 8 May 2021

Keywords:
Anderson type manganese polyoxomolybdate (POMo)
Organo-conjugate
Eudesmic acid (EU)
Apoptosis
Anticancer agent
Quantum chemical calculations

ABSTRACT

In this work, trimethylated gallic acid (Eudesmic acid, EU) was selected for the synthesis of an organo-conjugate (EU_2POMo) from TRIS modified Anderson-type manganese polyoxomolybdate (POMo) for the first time.

EU_2POMo was synthesized through amide bonding between POMo and EU using carbodiimide coupling strategy. Some of the quantum chemical properties of POMo and EU_2POMo beside the DFT and TD-DFT calculations were done using the Gaussian program. The cytotoxicity was studied on breast cancer cell lines (MCF-7 and MDA-MB-231) comparing the Human Umbilical Vein Endothelial Cell line (HUVEC) using the MTT method. The cellular uptake was determined using the ICP-MS method, and the apoptosis value was checked by the flow cytometry technique on the MDA-MB-231 cell line.

The structure was approved by FTIR, NMR spectroscopy as well as elemental analysis. Quantum chemical calculations proposed better stability and lower chemical potential for EU_2POMo, and internal energy and dipole moment were higher in the EU_2POMo. Both POMo and EU_2POMo showed reasonable anti-cancer effects on breast cancer cell lines (MCF-7 and MDA-MB-231), and the results were somewhat in favor of POMo. Interestingly, EU_2POMo showed no significant cytotoxicity on the HUVEC and was safer than POMo. Cellular uptake (33.5% versus 29.2%) and apoptosis value (28% versus 15%) in the case of EU_2POMo were slightly better than POMo.

In conclusion, this study aimed to introduce a novel, potent and safe anti-cancer Anderson type polyoxometalate to cancer studies. Based on results, this conjugate has sufficient potential for further cancer chemotherapy assessments, specifically breast cancer.

1. Introduction

Cancer is an abnormal growth and uncontrollable cell division in a specific part of the body that rapidly spreads and hurts other organs and other tissues [1]. Breast cancer is one of the most commonly diagnosed cancers in women impacting 2.1 million women each year and causes the most considerable number of cancer-related deaths among them. Chemotherapy is the most interesting and the best applicable method for treatment in this regard. However, the general toxicity and side effects of non-selective function in these drugs (such as cisplatin, doxorubicin, etc.), drastically reduce patients' quality of life [2,3]. So the researchers always try to introduce new drugs with better potencies and minimized side effects on healthy cells.

Polyoxometalates (POMs) with well-documented activities in cancer treatment have gained significant interest in this context. POMs are a class of anionic clusters composed of transition metals in the highest oxidation state (W(VI), Mo(VI), V(V)), and oxygen atoms [4]. These metal-oxo clusters with variable physicochem-

* Corresponding author.
E-mail address: m.rostami@pharm.mui.ac.ir (M. Rostami).

https://doi.org/10.1016/j.molstruc.2021.130612
0022-2860/

ical features have emerged in different fields such as catalysis, nanoscience, macromolecular crystallography, and medicine [5,6].

The simple and inexpensive chemical preparation and modification make POMs valuable candidates as anti-cancer agents. Since Yamase's first study in 1988 [7] on the anti-cancer effects of POMs, to date, many research and review articles [8–13] have confirmed the anti-cancer activities of these compounds. Therefore, these compounds appear to have the potential to be considered as anti-cancer drugs clinically. However, one of the biggest problems in entering POMs into clinical evaluations is the high intrinsic toxicity of these compounds to normal cells and healthy tissues. Although this toxicity is still lower than many other anti-cancer drugs, the high IC_{50} about mM in POMs has made it difficult for these compounds to enter the clinic. Therefore, researchers in this field have always tried to reduce IC_{50}s besides lowering the toxic effects of these compounds.

Gallic acid (GA), as a naturally occurring phenolic structure, is well known for the high biological activity, such as antiviral and anti-cancer effects [14]. The cytotoxic effects of GA and its derivatives on various cancerous cell lines were approved [15]. Eudesmic acid (EU), the tri-methoxylated form of GA, as presents in colchicine (a tubulin inhibitor anti-tumor drug), is the most-studied mimetic moiety to dedicate the anti-cancer activity to a chemical structure. Notably, 3,4,5 tri methoxyphenyl (TMP) is a chief moiety in tubulin inhibitor anti-cancer drug structures, which induces intense anti-cancer activity [16].

Molecular hybridization has been well experienced as an effective strategy in medicinal chemistry [17], in most cases, the hybrid molecules emerge integrated biological effects of their sub-units. In this regard, different pharmacophores, organic or inorganic moieties, could be hybridized rationally to get the desired effects. It seems the hybridization could be an ideal strategy to control the inherent cytotoxicity of POMs [18,19] and make them more selective.

During the last decades, there are valuable reports on the anti-cancer activity of organic hybrid POMs [8,9] both in vitro and in vivo.

Some of these hybridization approaches, such as binding to amino acids, Biotin [20,21], tocopherol succinate [22], peptides [23], bisphosphonate [9], etc. have been pioneers in this regard. It should be noted that the modification through the covalent bonding is more interesting than physical or ionic hybridization because of better biological stability and more selectivity [8,19] of POMs conjugates.

Following our recent studies and interests, we aimed to evaluate the synergistic effect of the EU on the cytotoxicity of an Anderson type polyoxomolybdate (POMo). As explained, Eudesmic acid is found in the chemical structure of anti-cancer compounds, especially tubulin inhibitors, and therefore we expected that binding of EU to the POMo structure could enhance the anti-cancer effects of the hybrid conjugate. So, EU_2POMo conjugate was synthesized using an amide bonding strategy, and the cytotoxicity of this novel conjugate was studied on two types of cancerous cell lines beside the HUVEC normal cells by MTT assay. Furthermore, the value of the apoptosis pathway in cytotoxicity effect was studied quantitatively. As a complementary evaluation, to compare quantum chemical properties and stability of prepared conjugate (EU_2POMo) with the initial POMo, quantum chemical calculations and TD-DFT were done using the Gaussian program.

2. Experimental section

2.1. Materials

Sodium molybdate (Na_2MoO_4•$2H_2O$), Tetrabutylammonium bromide (TBAB), Eudesmic acid (EU), Manganese (II) acetate tetrahydrate, glacial acetic acid (GAA), N–Hydroxy succinimide (NHS), Tris(hydroxymethyl)aminomethane, 3-(4,5-dimethylthiazol-2-yl)−2,5-diphenyl tetrazolium bromide (MTT), 1-Ethyl-3-(3-dimethylaminopropyl) carbodiimide hydrochloride (EDC) were purchased from Sigma-Aldrich Company (Germany). The MCF-7, MDA-MB-231, and HUVEC cell lines were supplied by the Pasteur Institute (Iran). Trypsin/EDTA, Streptomycin/penicillin, FBS and RPMI 1640 were purchased from PAA Company (Australia). All of the other necessary materials and solvents were provided by similar sources and used without further purification.

2.2. Instrumentation

(^{1}H &^{13}C) NMR spectra were recorded on NMR (Bruker Biospin AC-80, 400 MHz, Germany) spectrometer with deuterated DMSO as solvents at 25 °C and chemical shifts have been recorded in ppm units relative to tetramethylsilane (TMS). Fourier-transform infrared (FT-IR) spectra (KBr pellet) were recorded on a FT-IR (6300, JASCO, Japan) instrument in the range of 350–7800 cm^{-1}. UV-Visible spectral analysis was carried out by use of UV-mini-1240, (Shimadzu, Kyoto, Japan) spectrophotometer. The absorbance of each well in MTT assay was measured using a microplate reader of Awareness Statfax 2100.

The cells were assessed using BD FACSCalibur flow-cytometer (Becton Dickinson, USA) and the FlowJo-V10 software was used to analysis of data. Elemental analyses (C, H and N) were conducted on a Elementar, Vario EL (III) CHNSO elemental analyzer, for this the sample was dried at room temperature under a vacuum of 10^{-4} mmHg overnight.

Mn, and Mo were determined by an inductively coupled plasma ICP-OES spectrometer (Perkin Elmer, Optima 7300DV). To determine the molybdenum content in cellular uptake, study was again carried out by Agilent 7800 ICP-MS.

2.3. Methods

2.3.1. Chemical synthesis of EU_2POMo conjugate

Synthesis of $(TBA)_4[\alpha\text{-}Mo_8O_{26}]$: Firstly, Sodium molybdate dihydrate (Na_2MoO_4• $2H_2O$) (5 g, 20.7 mmol) was dissolved in 12 mL distilled water, and the solution was acidified to pH 3 by HCl (6 N). The reaction mixture was stirred vigorously for several minutes then a solution of TBAB in water (3.34 g, 10.4 mmol) in 10 mL water was added to it. After stirring for 10 min, the white precipitate was filtered and washed successively with distilled water, ethanol, and diethyl ether. The product, a white powder, was dissolved in acetonitrile, and the colorless cubic crystals were obtained by keeping them at −10°C overnight. The product was dried under vacuum and stored for the final step (C) [24]. The elemental analysis was used beside the FTIR analysis for structure approval. Elemental analysis: calculated for $C_{64}H_{44}N_4Mo_8O_{26}$: C, 35.70; H, 6.74; N, 2.60; Mo, 35.64. Found: C, 35.62, H, 6.81; N, 2.56; Mo, 35.63.

Synthesis of Mn $(CH_3COO)_3.2H_2O$: A solution of Mn $(CH_3COO)_2$•$2H_2O$ in GAA (0.16 g/mL) was heated to 110°C, and 0.68 g of KMnO4 was added in small portions for 20 min. The reaction mixture was cooled, poured in water, and left to crystallize overnight. The brown product was air-dried and stored for the final step (C) [25].

Synthesis of $[N(C_4H_9)_4]_3[MnMo_6O_{18}\{(OCH_2)_3CNH_2\}_2]$(POMo): At the final step to get the POMo, a mixture of $(TBA)_4[\alpha\text{-}Mo_8O_{26}]$ (8 g, 3.7 mmol), Mn $(CH_3COO)_3$ .2H2O (1.49 g, 5.6 mmol), and TRIS (1.56 g, 12.8 mmol) in150 mL acetonitrile was refluxed for 16 h. The orange solution was filtered to eliminate any precipitates, the large orange crystals were obtained by ether diffusion of filtrate for a long time and dried under vacuum (8). The chemical structure was studied and approved by FTIR, and ^{1}H NMR spectroscopies as

well as by the elemental analysis by CHNS and ICP-OES methods [20]. The elemental analysis was used beside the ^{1}H NMR, FTIR, and UV–visible analysis for structure approval. Elemental analysis: calculated for $C_{56}H_{124}MnMo_6N_5O_{24}$: C 35.73%; H 6.64%; N 3.72%, Mn 2.92%, Mo 30.59%; found experimental C 35.73%; H 6.73%; N 3.62%, Mn 2.86%, Mo 30. 45%.

Synthesis of EU_2POMo: EU (0.4 g, 2 mmol) was activated by EDC/NHS (0.41 g, and 0.23 g respectively, 2 mmol) in dried acetonitrile for 24 h under N_2 atmosphere at room temperature. The resulting solution was filtered and was added into the solution of POMo (1.88 g,0.001 mol) in dried acetonitrile, and the reaction mixture was stirred for 24 h at room temperature to get EU_2POMo [26]. The final solution was first dried under reduced pressure to get the product and then washed thoroughly with the cold ethanol to get the purified product. The chemical structure was studied and approved by FTIR and (^{1}H, ^{13}C) NMR, UV-visible spectroscopy and complete elemental analysis by CHNS and ICP-OES methods. Elemental analysis: calculated for $C_{76}H_{146}MnMo_6N_5O_{32}$ (Mol.Wt: 2272.56 g/mol): C, 40.17; H, 6.48; Mn, 2.42; Mo, 25.33; N, 3.08; found experimental C, 40.08; H, 6.97; Mn, 2.47; Mo, 25.49; N, 3.18;

2.3.2. Computational method

The quantum chemistry calculations have been used to determine the geometry optimization and electronic structure of POMo and EU_2POMo. The geometry optimizations were performed at the B3LYP [27,28] level of theory. The 6–31 G basis set used for all atoms, and DGDZVP [29] for the Mn and Mo. All calculation calculated by Gaussian 09 program.

2.3.3. Stability of EU_2POMo

For this purpose, a solution of EU_2POMo (40 µg / mL) were prepared at pH=7.4 in PBS-1% DMSO. Upon mixing with PBS, the clear solution was retained. The solutions were scanned immediately, after 72 and after 96 h by UV–Vis spectrophotometer [30,31].

2.3.4. In vitro cell viability assay

Two types of breast cancer cell lines comprising MCF-7 and MDA-MB-231 beside the normal cell line (HUVEC) were selected for in vitro cytotoxicity evaluations. The cells were cultured at the standard condition of 10% fetal bovine serum (FBS) and 1% penicillin-streptomycin at 37 °C in an atmosphere of 5% CO2, then were retained in RPMI-1640 (GIBCO) medium for following cytotoxicity evaluation using MTT protocol [32]. Typically, stock solutions were prepared at a 500 μg/mL concentration in phosphate-buffered saline (PBS). Cells at a density of 5×10^3 per well were seeded, then incubated at the same condition as culturing step for 24 h. Various concentrations of the test groups (POMo, and EU_2POMo) ranging from 25, 50, 100, 200 μg/mL were treated regularly on MCF-7, MDA-MB-231, and HUVEC Cells plates. After incubation for 72 h, the medium was removed, and 20 µL of MTT solution (5 mg/mL) was added to each well, and incubation was continued for 4 h. After that, the medium was replaced with 150 µL DMSO to solubilize the purple formazan precipitates, and the absorbance was read using a microplate reader at 570 nm. The cell viability was calculated using the following equation [33];

$$\text{Cell Survival \%} = \frac{(A_t - A_b)}{(A_c - A_b)} \times 100 \quad (1)$$

in which A_t, A_b and A_c represent mean absorbance of the treatment, blank and negative control, respectively [34]. For each treatment, the average of 9 runs were considered, and results were given as Mean ± SD.

2.3.5. Flow cytometry analysis of cell apoptosis

To verify the apoptosis pathway, briefly, MDA-MB-231 cells were seeded in a 12-well plate with a density of 10^4 cells/well and incubated for 24 h at 37 °C. POMo and EU_2POMo solutions with a 200 μg/mL concentration were treated on cells, and incubation was followed for the next 24 h at the same condition. After that, the cells were washed three times with cold PBS and then harvested using Trypsin. The apoptosis rate was detected according to the operation steps of the Annexin V-FITC PI (Propidium Iodide) apoptosis assay kit (IQ product, Netherlands) in the dark for 15 min at room temperature. The apoptosis level was determined using FACS Calibur flow cytometer, and just the single cells were gated for fluorescence analysis [35].

2.3.6. Cellular uptake analysis

The cellular uptake of EU_2POMo in comparison to POMo was checked on the MDA-MB-231 cell line by ICP-MS. The MDA-MB-231 breast cancer cells were grown in flasks at 37 °C in a 5% CO2 atmosphere until at least 70% of confluency. The medium was removed and replaced with 14 mL RPMI-15% FBS and 1% DMSO containing 90 μg/mL concentration of POMo, and EU_2POMo. After 24 h incubation time at mentioned condition, the medium was removed, and the cells were washed with 10 mL PBS then detached by trypsinization and re-suspended in 10 mL PBS (pH 7.4). The suspension of cells was centrifuged (2000 rpm, 5 min), and the isolated pellets were washed twice with ice-cold PBS. The isolated pellets were re-suspended in 500 µL deionized water (cells were counted before lysis) and the cells lysed using a sonotrode. For protein determination by the Bradford method, an aliquot of each lysate samples was stored at −20 °C. The lysates were stabilized by the addition of 15 µL of HNO_3 (10%)–HCl (30%) and 15 µL of Triton X-100 (1%) for their molybdenum content determination by ICP-MS. The cellular concentration of Mo was expressed as µg per each mg of cellular protein [12, 36].

2.3.7. Statistical analysis

All data were analyzed using one-way ANOVA using SPSS software (the version of 21) followed by student *t*-test to evaluate the difference between groups or by Post Hoc LSD test for more than two groups. The p-value lower than 0.05 was considered as a significant difference between averages.

3. Results and discussion

3.1. Synthesis of EU_2POMo

Eudesmic acid is known as the trimethylated derivative of gallic acid, which has been considered a significant component in the structure of tubulin inhibitor compounds in the field of medicinal chemistry [14]. This structural component is found in known molecules such as combretastatin A4, podophyllotoxin, colchicine, and phenstatin, which can bind to the colchicine acceptor site [15]. For this reason, the participation of this structural part in molecular designs based on the structure-reactivity relationship in the tubulin polymerization inhibition strategy is well known and usually leads to the improvement of anticancer activities in the final compounds. Therefore, the binding of this moiety to the Anderson-type manganese polyoxomolybate seemed to be a powerful strategy in designing a cytotoxic agent.

In recent years, Anderson-type polyoxometalate compounds have received much attention with the possibility of inserting TRIS-like groups into them [37], which can provide suitable functional groups for modifying the structure of polyoxmetalates. Among these, Anderson-type manganese polyoxomolybdate has been considered by many research groups for different purposes. This polyoxomolybdate has shown good anticancer properties, and in numerous evaluations, its hybrid structures have provided new efficiencies and capabilities.

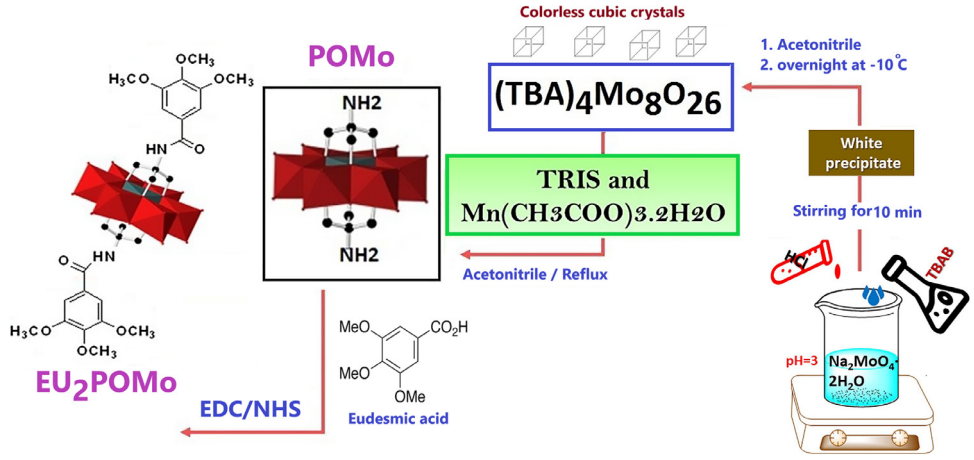

Fig. 1. Chemical procedure for synthesis of EU_2POMo from Na_2MO_4.

With these explanations and following our recent studies [22,38], we aimed to achieve synergistic effects by synthesis a new cytotoxic compound from hybridization eudesmic acid with Anderson-type manganese polyoxomolybdate (POMo).

For this purpose, $[TBA]_4[\alpha\text{-}Mo_8O_{26}]$ was synthesized simply according to the earlier reports as the essential core of POMo. After the addition of $Mn(OAc)_3$ and TRIS to $[TBA]_4[\alpha\text{-}Mo_8O_{26}]$, $[TBA]_3[MnMo_6O_{18}\{(OCH_2)_3CNH_2\}_2]$(POMo) was isolated as orange crystals in 80% yield [39]. The reaction of POMo with 2 moles of EU gives in hand the final conjugate EU_2POMo as a pale orange powder (Fig. 1). Based on available sources, in the chemical scaffold of manganese Anderson type polyoxomolybdate, six edge-sharing octahedral MoO_6 units arrange themselves around a core of the MnO_6, build an Anderson type structure. The TRIS moieties are inserted into the scaffold via its alkoxy groups on the Mn (III) ion; in this manner, two amine groups of TRIS are oriented outwards and are available for further modification of POMo. The organic molecules can cover both sides of the planar hexagon polyoxomolybdate structure via the chemical bonding with amine groups of TRIS symmetrically or unsymmetrically [39].

As shown in Fig. 1, we utilized both amine groups of POMo for the conjugation to the EU. The amidation reaction between EU and POMo was carried out through the carbodiimide strategy using EDC/NHS reagents [40]. Purification through precipitation and recrystallization yields the pure final product in an almost quantitative yield.

3.2. Computational assessments

The chemical structure of POMo and EU_2POMo conjugate was optimized using Gaussian software protocols, and also, some physicochemical properties were studied using quantum chemical calculations. These results helped us to have a prediction on some of the structural features and reactivity.

The optimized geometries of EU_2POMo and POMo, obtained by the Gaussian 09 program, are presented in Fig. 2. The geometry optimizations were performed at the DGDZVP level for Mo atoms and B3LYP/6–31 G level for all others atoms. The obtained ΔU° values were compared to examine the stability of POMo and EU_2POMo related structures. The more negative the ΔU° level of a compound, the more stable it is. Table 1 shows the ΔU_f°, ΔH_f° and ΔG_f° for POMo and EU_2POMo, as can be seen, the internal energy is in the order EU_2POMo < POMo. Therefore, the EU_2POMo conjugate is about twice more stable than the initial POMo; these results are in good agreement with those obtained by Schönweiz et al. [41], at least in the case of POMo.

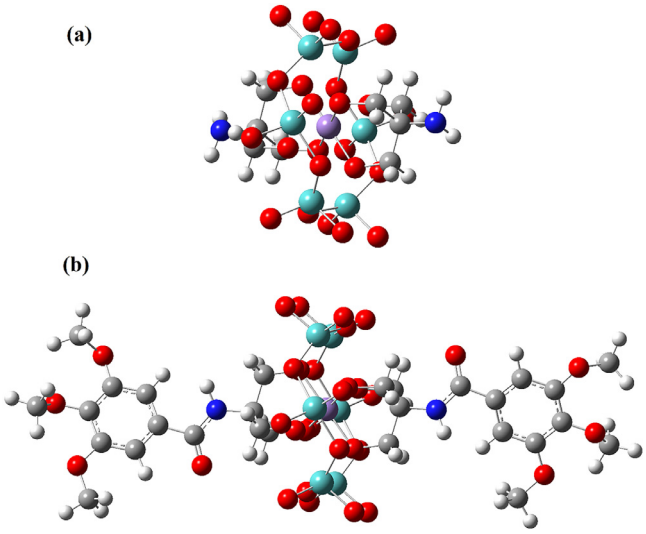

Fig. 2. The optimized geometries of a: POMo and b: EU_2POMo.

Table 1
The Thermodynamic energies ΔU°_f, ΔH°_f and ΔG°_f of POMo and EU_2POM species at B3LYP/6–31G-DGDZVP level of theory (6–31 G basis set for C, N, O, H atoms and DGDZVP basis set for Mn & Mo atom).

Compounds	ΔU°_f / eV	ΔH°_f / eV	ΔG°_f / eV
POMo	−375.321	−376.749	−355.991
EU_2POMo	−646.204	−648.856	−610.923

The electric dipole moment (μ_0) is an essential molecular parameter that plays an essential role in dipole-dipole interactions and other applications in solids and liquids. Table 2 shows the calculated values of μ_0 (in Debye) for POMo and EU_2POMo; according to Table 2, the dipole moment of EU_2POMo is more significant than that of POMo. The higher dipole moment in EU_2POMo causes EU_2POMo to dissolve more in polar solvents and interact more with water and polar liquids.

The molecular orbital theory is used routinely to determine the stability and activity of molecules. Various values such as HOMO-LUMO gap (E_{gap}), global hardness (or chemical) (η), chemical potential (μ) and electrophilicity (ω) can be calculated in this framework [42]. These values can be calculated from the following equations using the highest occupied molecular orbital (HOMO) and the

Table 2
Energies of HOMO and LUMO, HOMO-LUMO energy gap (E_{gap}), chemical hardness (η), chemical potential (μ), electrophilicity (ω) and dipole moment (μ_0).

Compounds	E_{HOMO}/eV	E_{LUMO}/eV	E_{gap}/eV	η/eV	μ/eV	ω/eV	μ_0 / Debye
POMo	1.169	3.925	2.755	1.377	−2.547	4.468	1.569
EU_2POMo	0.791	3.539	2.748	1.374	−2.165	3.222	4.196

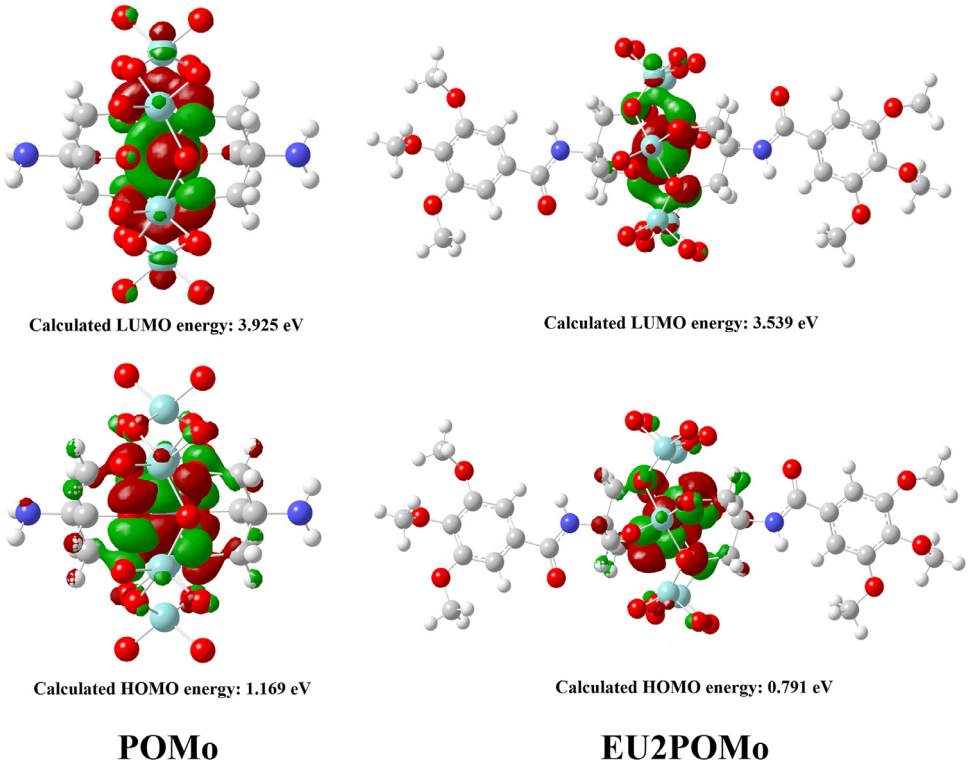

Fig. 3. Topology of HOMO & LUMO orbitals for POMo and EU_2POMo.

lowest unoccupied molecular orbital (LUMO).

$$\eta = \frac{(E_{LUMO} - E_{HOMO})}{2} \quad (2)$$

$$\mu = -\frac{(E_{HOMO} + E_{LUMO})}{2} \quad (3)$$

$$\omega = \frac{\mu^2}{2\eta} \quad (4)$$

Table 2, shows the calculated HOMO, LUMO, η, μ and ω for POMo and EU_2POMo. According to this table, the energy of the gap (HOMO-LUMO) in EU_2POMo is slightly larger than that of POMo. Also based on the Table 2, the chemical potential of EU_2POMo is greater than that of POMo which would be a great prediction for reactivity of EU_2POMo compare to the POMo. The spatial distributions of HOMO and LUMO molecular orbitals for POMo and EU_2POMo, besides the calculated energy levels, are shown in Fig. 3. According to these shapes, we find that the shape of these orbitals is almost the same for both compounds, and that in both compounds, the major orbital density is concentrated on the central core of the POMo.

In the following section, the characterization of the EU_2POMo structure will present beside the predicted data to approve the successful chemical synthesis of EU_2POMo.

The structure of POMo has been constructed in two steps, as described earlier and due to the existence of numerous valid reports for this structure, only FTIR, ^{1}H NMR, and elemental analysis results were checked and verified with comparison to standard samples [38, 39]. Spectral data for $[TBA]_4[\alpha\text{-}Mo_8O_{26}]$ and POMo are provided as follow:

$[TBA]_4[\alpha\text{-}Mo_8O_{26}]$; FTIR (KBr): ν (cm^{-1}) (500–1000 cm^{-1}), 954 (m), 942 (m), 923, (Mo=O, vs), 912 (vs), 906 (s), 852 (m), 807 (vs), 664 (vs), 560 (m).

$[TBA]_3[MnMo_6O_{18}\{(OCH_2)_3CNH_2\}_2]$ (POMo); FTIR (KBr): ν (cm^{-1}), 3448 (N–H str., br), 2960 (C–$H_{str.}$, s), 2934 (C–$H_{str.}$, s), 1608 (N–$H_{def.}$, w), 1479 (s), 1381 (m), 1040 (s), 939 (s, Mo=O), 917 (s, Mo=O), 900 (s, Mo=O), 663 (s, Mo-O-Mo); ^{1}H NMR (400 MHz, DMSO-*d6*): 0.94 (t, 36 H), 1.32 (m, 24 H), 1.57 (m, 24 H), 3.12 (m, 24 H), 61.8 (s, 12 H); UV–Vis. (CH_3CN): λ_{max}, 216 nm (O^{2-} to Mo^{6+} charge transfer) [23].

The structure of **EU_2POMo** was characterized by FTIR spectroscopy (Fig. 4-left), UV-visible spectroscipoy (Fig. 5-down), ^{1}H NMR spectroscopy (Fig. 6-up), ^{13}C NMR (Fig. 6-down), and complete elemental analysis (using CHNS & ICP-OES), the results are as follow:

EU_2POMo conjugate; FTIR (KBr): ν (cm^{-1}) 3324 (w, br), some medium weight bands below 3000 cm^{-1}, 1632.38 (m, amide C=O of EU), 1479 (m), 1041 (s), 939 (s, Mo=O), 917 (s, Mo=O), 900 (s, Mo=O), 663 (s, Mo-O-Mo). ^{1}H NMR (400 MHz, DMSO-*d6*): 1.07 (t, 36 H, POMo), 1.33–1.35 (m, 24 H, POMo), 1.5–1.8 (m, 24 H, POMo), 3.23 (m, 24 H, POMo), 7.33 (d, J = 4.4, H Ar. EU), 8.53 (bs, 2H, newly formed amide NH), 62.20 (s, 12 H, POMo); ^{13}C NMR (100 MHz, DMSO-*d6*): 175.37 (C=O), 152.75 (=C-OMe, meta-position), 143.06 (=C-OMe, para-position), 137.64 (=C-C=O), 123.17 (=C-H), 84.99 (-CH_2–O (TRIS)), 74.32 (N–C(TRIS), 60.19 (-N^+-CH_2-),

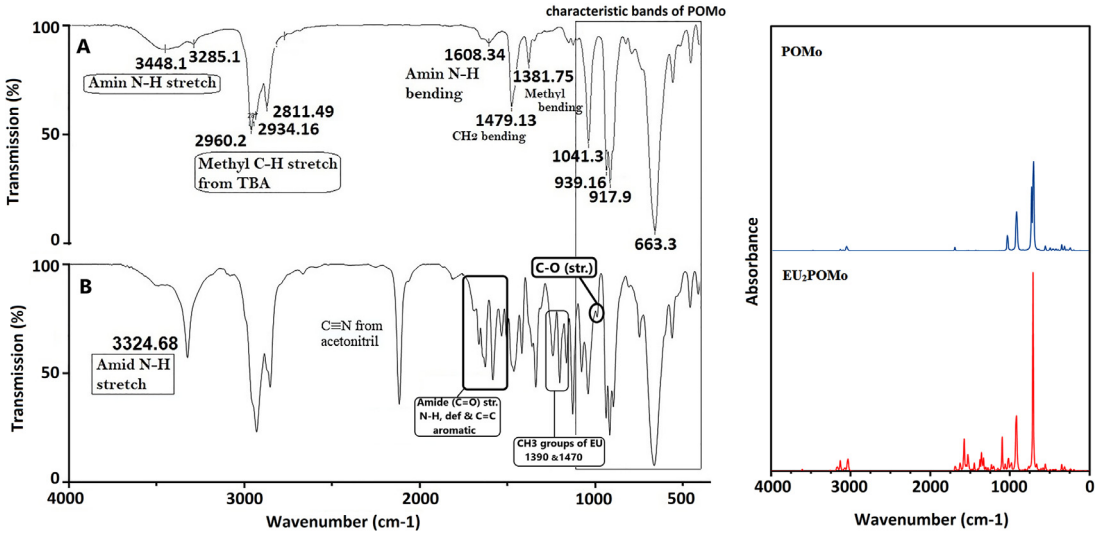

Fig. 4. Experimental FTIR (Left) & Predicted IR (Right) spectrums for POMo & EU_2POMo.

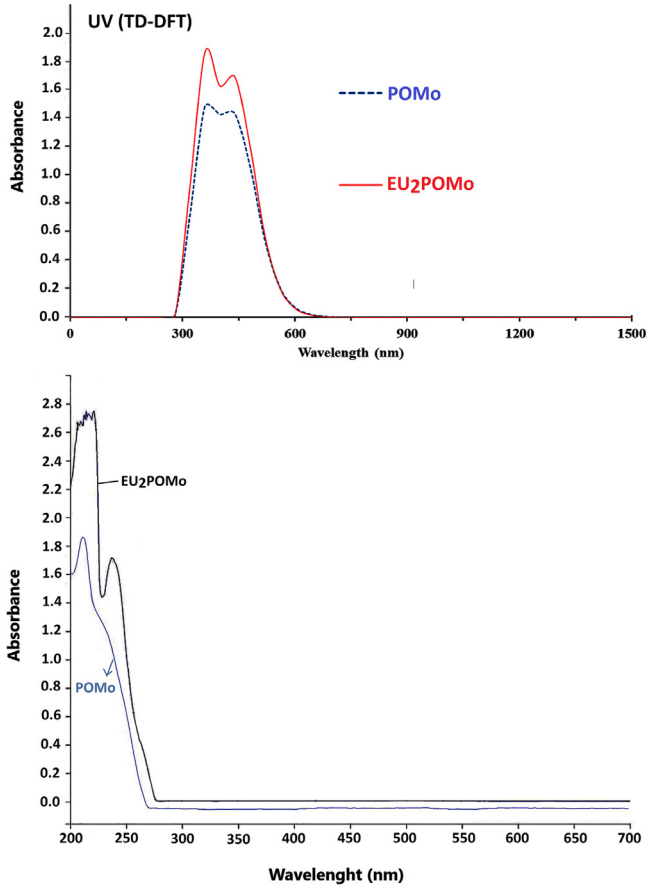

Fig. 5. Experimental (down) & Predicted UV spectrum (up) for POMo & EU_2POMo.

56.10 (=C–OCH_3), 24.84 (CH_2, TBA), 20.72 (CH_2, TBA), 13.89 (CH_3, TBA). UV-Vis. (CH_3CN): 214 (λ_{max}), 235 nm.

Infra-red spectra: The theoretical IR spectra for two components POMo and EU_2POMo conjugate, were predicted from the above-mentioned Gaussian calculations and shown in Fig. 4 (right). Compare to the POMo, EU_2POMo has additional bands related to the aromatic segments above 3000 cm^{-1} and in the range of 1000–1800 cm^{-1} beside the original POMo characteristic bands with greater intensities. The POMo has a maximum absorption at the frequency of 705 cm^{-1}, but the EU2POMo has maximum absorption at a wavenumber of 709 cm^{-1}; these wavelengths are related to the Mo-O bond stretching frequencies. Adding the aromatic rings causes the absorption to shift to the higher wavenumbers and the intensity of absorption increases. The change in higher wavelengths and increasing absorption intensity for EU_2POMo is logical because of the addition of aromatic rings, increases the μ_0 (dipole moment), and the intensity of absorption per frequency is proportional to the μ changes. Due to the more significant dipole moment (μ) in the EU_2POMo, this compound has a higher adsorption intensity than the POMo. As will discuss in the following section, there is a similar pattern for experimental conditions for comparing POMo and EU_2POMo IR spectra.

With an in-depth look at the experimental FTIR spectrum (Fig. 4-left) of the final conjugate compare to the POMo, we find some changes after the conjugation. For example, N–H stretching frequency has somewhat decreased from 3448 cm^{-1} to 3324.7 cm^{-1}, the carbonyl group stretching frequency has been added to spectra with a change in location from 1719 cm^{-1} in EU to the lower wavenumbers around 1632–1680 cm^{-1} in EU_2POMo due to the conjugation, this spectral area is the characteristic feature of aromatic amide conjugates. Furthermore, those characteristic features of EU moiety, specifically benzene ring (CH stretching vibration), has emerged their properties in the FTIR in the region of >3000 cm^{-1}. Similarly, an increase in the intensity of bands before 3000 cm^{-1}, which belongs to CH_3 group stretching modes, again approves the presence of EU moiety. Finally, those vibrations around 1390 and 1470 cm^{-1} could be related to the CH_3 group vibrations; furthermore, ν_{C-O} around 1030 cm^{-1} attest to the binding of the EU ligand to the POMo core. Furthermore, we have some additional bands related to EU around the 1500–1650 cm^{-1} region (stretching and deformation modes of C=C, N–H bonds vibrations). Furthermore, we can see the characteristic bands of Anderson-type POMo at proper regions after conjugation with EU, these uniquely strong representative bands for Mo_6O_{18} core were located in 1041, 939, 917, and 663 cm^{-1}, the $\nu_{Mo=O}$ band at 663 cm^{-1}, and $\nu_{Mo-O-Mo}$ at 939, 917 cm^{-1} are characteristic of the Anderson structure [39]. These IR proofs, which are in excellent agreement with calculated spectra (Fig. 4-right), undoubtedly convinced us of the correct amide formation between EU and POMo.

UV-visible absorption spectrum and TD-DFT calculations; the TD-DFT calculation was performed using Gaussian (the B3LYP / 6–

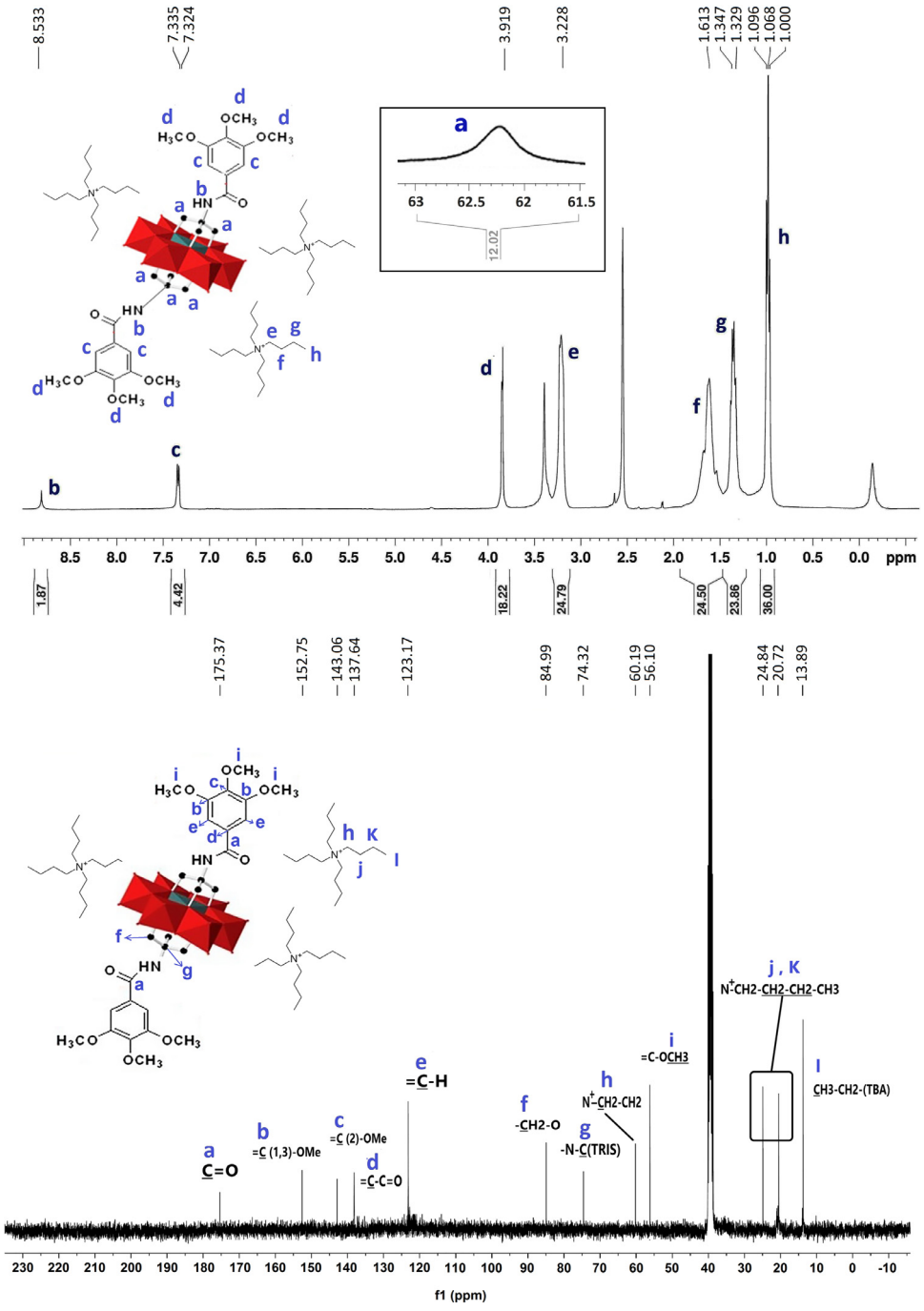

Fig. 6. ^{1}H NMR spectra (up) & ^{13}C NMR spectra (down) for EU_2POMo conjugate.

31 G method) to estimate the electronic transitions of POMo and EU_2POMo as UV spectra, and the results are shown in Fig. 5(up). According to the calculated UV–Vis spectrum, which corresponds to both compounds (POMo & EU_2POMo), a doubled broad peak is seen at a distance of 300–600 nm in the gas phase studies. These peaks consist of the overlap of two peaks, the maximum of which occurs between 365 (2.9 eV) and 425 nm. These peaks can be related to the electronic transition from the HOMO to LUMO and HOMO-1 to LUMO+1. Due to the small distance between these levels (Table 2), these peaks have overlapped. The first peak at λ_{max} = 365 nm is comparable to the difference gap between HOMO and LUMO (HOMO-LUMO = 2.75 eV) and probably belongs to a charge transfer from O to Mo.

The experimental UV-visible spectrums of EU_2POMo and POMo were recorded in acetonitrile as the solvent, and results have been provided in Fig. 5-down besides the theoretical spectrums.

As it can be seen, POMo has a significant absorption at 216 nm, and in this regard, as the Figure depicts, there are some slight changes in the general profile of EU_2POMo. For EU_2POMo, the basis band for charge transfer from O^{2-} to Mo^{6+}has been retained with a slight displacement, and another apparent broadband related to the aromatic segment (π to π^*) which could be reasonably related to EU moiety, has been added to the diagram around 240 nm [24,43]. Ventura et al. reported the same results for their Bombesin-analog peptide conjugate with POMo [23]. By comparing the calculated UV-visible spectrum with that obtained exper-

imentally, some results are obtained. Firstly, the electronic transitions in the gas phase occur in longer wavelengths than the solution phase (experimental results); secondly, some electronic transitions seem to be mixed and altered to have resulted in spectral appearance changes in the solution phase. It is important to note that this comparison should be made with great caution, as LUMO and HOMO molecular orbitals, which are our benchmarks for electron transfers, are located on the inorganic core based on DFT calculations (Fig. 5-up). So, specifically for EU_2POMo, it is needed to have more information to conclude about electron transfers, and transfers between other orbitals should be considered carefully. It should be noted that in all theoretical calculations toward predicting the IR, UV, and NMR, the TBA cations have not been considered.

NMR studies; the (^1H, ^{13}C) NMR experimental spectra of EU_2POMo conjugate are the best complementary data. Fig. 6-up shows the ^1H NMR of the EU_2POMo conjugate as it can be seen all fundamental signals of TBA (signals between 1.0–3.5 ppm, 1, 1.3, 1.6, 3.2, and 3.9 ppm)), and TRIS (62–62.5 ppm) in the POMo scaffold are relocated intact in EU_2POMo conjugate. As shown by Marcoux et al. [39], due to the strong electron-withdrawing identity of POMo, its methylene protons (belong to TRIS) have appeared at a highly downfield area around 63 ppm in ^1H NMR with the correct signal ratio. Furthermore, the related signals of EU were correctly appeared in the correct regions, as shown in Fig. 6-up about 7.3 ppm (d, $J = 4.4$ Hz, H_C), and 8.5 ppm (N–H amide) with correct signal ratio to the other parts of spectra. Based on the ^1H NMR results, a newly appeared signal of amide (N–H, 2H) around 8.5 ppm, besides the correct ratio of aromatic signals of EU (7.3 ppm, 4H) to the TRIS around 62.2 ppm (12 H), confirmed the conjugation of 2 molecules of EU to the POMo.

Additional confirmatory information was extracted from the 13C NMR spectrum. In the carbon-13 spectrum shown in Fig. 6-down, four groups of signals are of great importance, the signals of the TBA cations appearing in the aliphatic carbons range and below the 60 ppm region. Aromatic signals appear in the area between 120 and 153 ppm, TRIS signals with two types of carbons appearing in the range of 74–85 ppm, and finally, the carbon amide signal appearing in the 175 ppm region. The two main changes expected in the spectrum are the addition of aromatic carbon signals to the related region and the emergence of carbon amide signal in the downfield area around 175 ppm.

The type of carbons and the intrinsic symmetry of the molecule are well inferred from the observed spectral design, as previously reported by Zhang et al. [44] for the chalcone amide conjugate, Sullivan et al. [45], and Li et al. [46] for related polyoxomolybdate conjugates.

By examining the predicted magnetic resonance spectrum of the EU_2POMo conjugate via quantum chemical calculations using the GIAO protocol and comparing the results with the results of the experimental section, RMSD values higher than five were obtained. Such results are always expected because studies run in the gas phase, and the solution phase parameters are not included in the calculations. So, the fundamental differences between predicted and experimental NMR data arising from differences between the gas and solution effective parameters. Furthermore, these differences may cause by differences in the structural constraints in two different phases [47].

In general, from comparing the predicted and experimental spectra, a suitable consistency is inferred between the two experimental parts and the theoretical calculations.

Finally, the complete elemental analysis data for the percentage of carbon, hydrogen, nitrogen, manganese and molybdenum obtained using CHNS and ICP-OES techniques showed an excellent agreement with the predicted cases for conjugate chemical structure. Two molecules of EU indeed have been attached to the POMo in EU_2POMo conjugate, signal ratios in ^1H NMR spectra, elemental CHNS analysis beside ICP-OES data approved this fact. The results of all the characterization techniques convinced us that the proposed conjugate structure was synthesized correctly.

Table 3
Comparative cytotoxicity of POMo & EU_2POMo on MCF-7 & MDA-MD-231 cell lines in different times.

Name of sample	Cell line	Time incubation (h)	IC_{50}(μg/mL)
POMo	MCF-7	48	303.82 ± 2.14
		72	161.5 ± 1.25
	MDA-MB-231	48	338.53 ± 2.31
		72	194.33 ± 1.02
EU_2POMo	MCF-7	48	330.43 ± 1.89
		72	194.7 ± 0.98
	MDA-MB-231	48	346.89 ± 1.67
		72	218.6 ± 1.13

3.3. Stability of EU_2POMo conjugate

The covalentley modified organo-POMs conjugates either through the in situ formation or post- functionalization, offers unquestionable benefits comprising; promising synergistic effects and better long-term stability both in solid and in aqueous media. In this regard, the stability of EU_2POMo conjugate before any further study and application should be analyzed [48, 49].

The UV/vis spectrum of EU_2POMo in PBS (Fig. 7) clearly indicates its stability around neutral pH conditions through monitoring of the characteristic POMo absorption bands, i.e. the characteristic EU_2POMo absorption bands did not undergo significant changes at any wavelength over a period of 4 days. These results agree well with the previously observed stability which was reported by Geisberger et al. [36].

3.4. In vitro *cytotoxicity assessments (MTT assay)*

To study the effect of EU conjugation on the cytotoxicity profile of POMo in final product, two cancer cell lines comprising MCF-7 and MDA-MB-231 were selected. The cells were treated with different concentrations ranging from 25 to 400 μg/mL of both POMo and EU_2POMo in the initial evaluation trial at different time of incubation (Table 3). Comparing the results in Table 1 shows that with increasing the incubation time, the cytotoxicity of POMo and EU_2POMo increases in both cell lines. For this reason, 72 h of incubation time, and concentrations range from 25 to 200 was chosen for further evaluation.

The results of *in vitro* cytotoxicity for the EU_2POMo in comparison to the POMo, on the MCF-7, and MDA-MB-231 was provided in Fig. 8. Based on this diagram, and cytotoxicity data which are provided in Table 3, the cytotoxicity profile is fully time and dose responsive ($p<0.05$ for each comparing). Eventually, Fig. 8c represents the comparative cytotoxicity of POMo and EU_2POMo on the HUVEC normal cells.

Previous reports have repeatedly referred to the potential activity of EU as Gallic acid trimethyl ether derivative to introduce anti-cancer properties in those structures that bearing this moiety. In this regard, the synergistic effects of the EU for inducing the cytotoxic properties in tubulin polymerase inhibitors [15] have been studied several times. So it seemed that the EU could be the right candidate for enhancing the anti-cancer properties of POMo.

As can be deduced from Fig. 8a, POMo and EU_2POMo exhibited considerably better growth inhibition effects on MCF-7 cell line. The IC_{50} of the POMo and EU_2POMo on MCF-7 cell line were 146.38 μg/mL, and 194.68 μg/mL respectively. On the other hand, both of POMo and EU_2POMo showed somewhat less cytotoxic effects on MDA-MB-231 cell line (Fig. 8b), the IC_{50}s were respectively

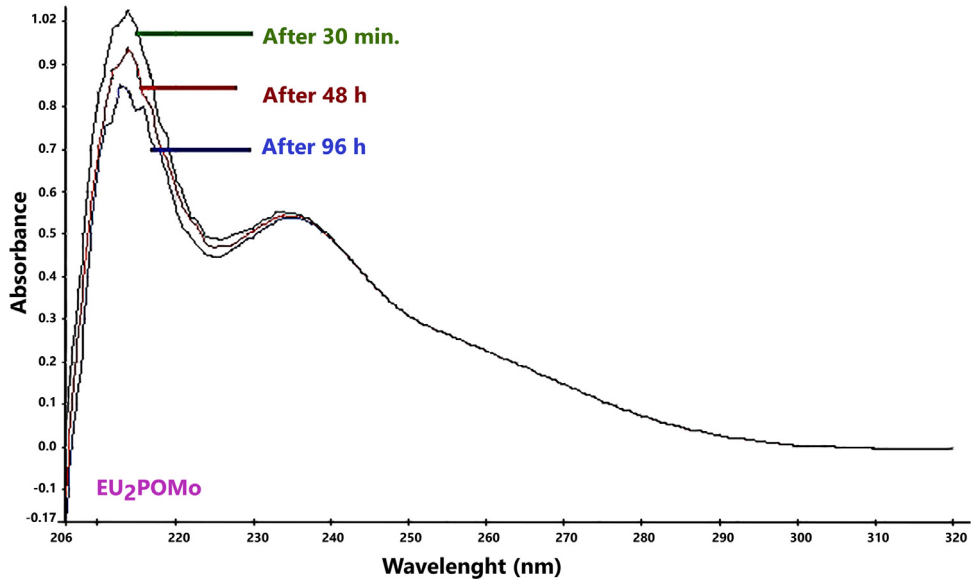

Fig. 7. UV–Vis. Spectra for EU_2POMo during stability assessments after 30 min. 48 h, and 96 h follow up.

Table 4
Cellular uptake quantity of POMo and EU_2POMo on MDA-MB-231 cell line based on Mo content determined by ICP-MS method.

Sample	The total quantity of sample in contact with the cells	Total protein(mg)	Mo total content in 90 μg of sample	Mo(µg/mg protein)	Uptake percent regarding total Mo content
POMo	90 µg/mL	4.6	28.09	8.2	29.2%
EU_2POMo	90 µg/ mL	4.1	23.26	7.8	33.5%
Control	–	5.0	0	0	0

156.80 μg/mL and 225.71 μg/mL for POMo and EU_2POMo in MDA-MB-231 cell line. The lower toxicity of the POMo and EU_2POMo on the MDA-MB-231 cell line can be attributed to the specific conditions and different intracellular pathways of this cell line and perhaps to the higher resistance of the MDA-MB-231 cell line to various therapies. Based on the results, the addition of the EU moiety to the POMo structure could not help improve the toxicity effects of this compound; however, the obtained IC_{50} is still in the range of reported values for this type of compound [10].

The second hypothesis of this study was to reduce the cytotoxicity effects on HUVEC normal cells, which is confirmed by the results of normal cell line (Fig. 8c). The cytotoxicity of EU_2POMo and POMo were evaluated on the HUVEC cells at the concentrations ranging from 25 to 200μg/mL. The EU seems to have protective effects and help to reduce the toxicity on the normal cell line. Interestingly, we did not get any considerable cytotoxicity on HUVEC for EU_2POMo compared to the POMo at the same concentrations. At concentrations above 50 μg/ ml, EU_2POMo is significantly safer than POMo, which can even alleviate the problem of higher IC_{50} of this compound. It seems that we can introduce EU_2POMo as a safe cytotoxic organo-polyoxometalate, the same results were reported for other hybrid organic-inorganic POMs [18,22].

3.5. Cellular uptake study

The Cellular uptake of POMo and EU_2POMo was evaluated comparatively on MDA-MB-231 cells by ICP-MS analysis (Table 4) based on the procedure reported by Geisberger in 2013 [36]. Control experiments without POMo did not display any Mo above the analytical detection limits, i.e., background concentrations in cells can be excluded.

After exposing to 90 mg/mL of POMo and EU_2POMo, however, molybdenum contents of MDA-MB-231 cells sharply raised to 7.8 and 8.2 μg per each mg of protein, respectively for POMo and EU_2POMo. On the other hand, the total quantity of Mo in POMo and EU_2POMo are different based on the structural formula and are 28.09 and 23.26 mg for POMo, and EU_2POMo respectively. Considering this fact, we can conclude that the cellular uptake of EU_2POMo is reasonably higher than the POMo. It seems that adding EU to the structure can improve the cell interactions and facilitates the entry [18].

3.6. Apoptosis quantification using flow cytometry protocol

To quantify the cell apoptosis, MDA-MB-231 cells (this cell line is routinely resistant to therapy) were treated with the same concentration of POMo and EU_2POMo (200 μg/mL). After incubation for 24 h, the cells were analyzed by Annexin V/propidiumiodide (PI) kit to determine the apoptosis quantity based on the protocol provided by the company. The Annexin V binds to cells in the early apoptosis stage, which can be used as a very specific apoptotic marker, and PI stains cells in late apoptosis and dead cells [35].

The results have been presented in Fig. 9; the upper left quadrant shows the percent of necrosis in cell death, the upper right shows late apoptotic cells, the lower left shows normal alive cells, and the lower right quadrant shows the cells in the early apoptosis stage. The results showed that the proportion of apoptotic cells (in the early and late phase) increased with POMo and EU_2POMo to 15% (total early and late apoptosis), and 28% (total early and late apoptosis) and 28%, respectively. The proportion of early apoptotic cells induced by the EU_2POMo is significantly higher than the POMo and more profoundly increased regarding the control group. So, it can be concluded that the conjugation of EU to the POMo improved the apoptosis value in cytotoxicity effect on the MDA-MB-231 cell line.

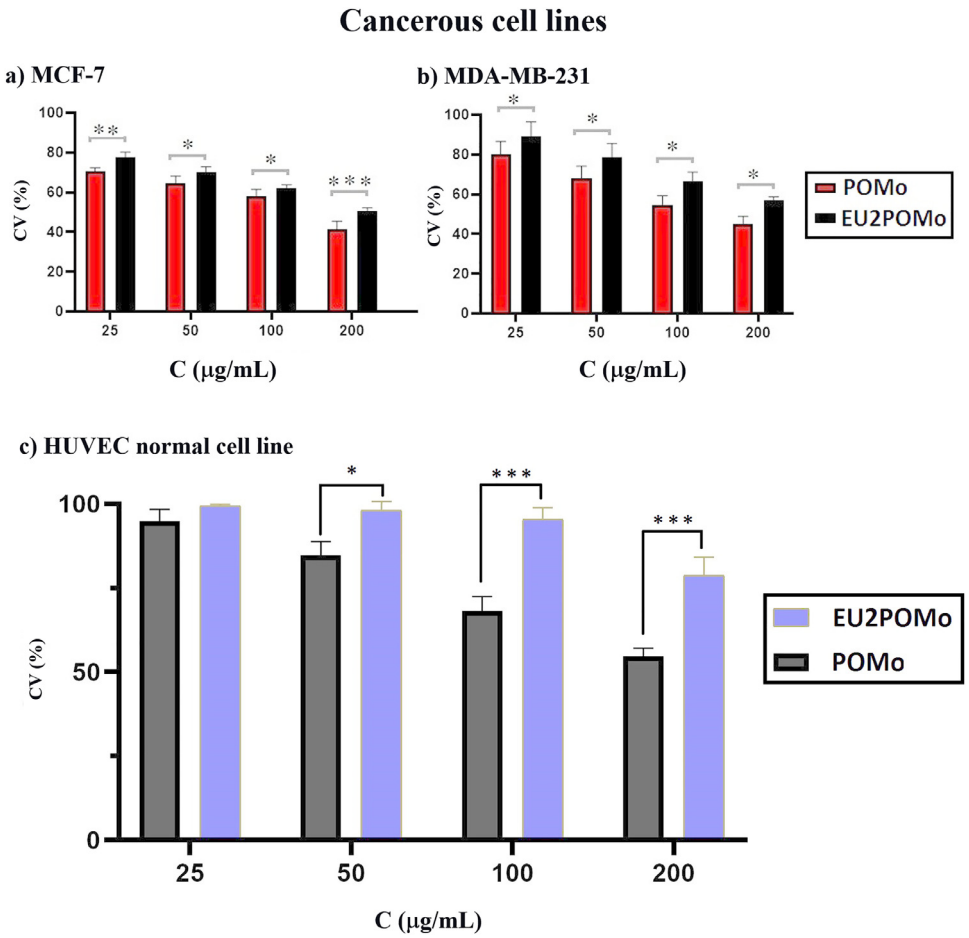

Fig. 8. The comparative cytotoxicity of EU_2POMo and POM on the a) MCF-7 & b) MDA-MB-231 cancerous cell lines and c) HUVEC normal cell line In each diagram * refers to significant difference $p<0.05$, ** refers to significant difference $p<0.01$, and *** refers to significant difference $p<0.001$.

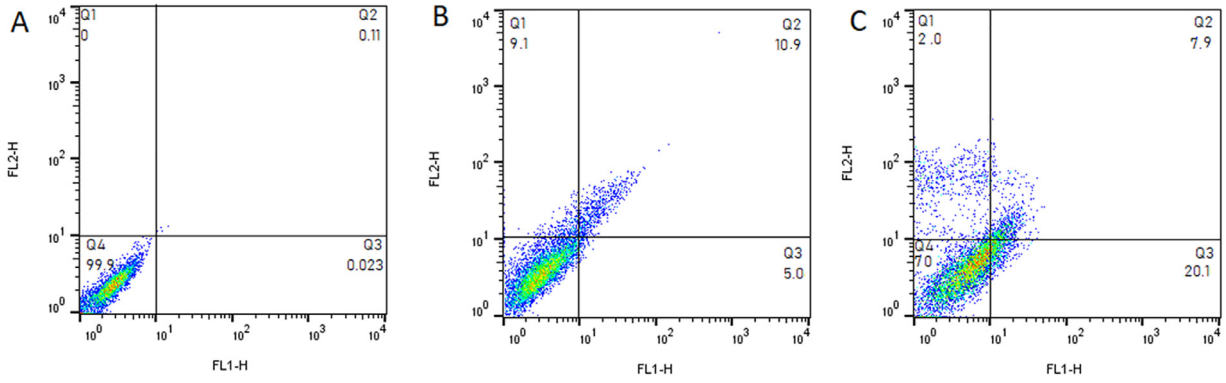

Fig. 9. Annexin V/PI analysis of apoptosis in MDA-MB-231 cancer cells induced by (A) Control; (B) POMo & (C) EU_2POMo.

The question may arise as to why EU_2POMo had less cytotoxic effects than POMo, given the higher cellular uptake and a higher percentage of apoptosis. It seems important to note that the higher percentage of cells in the early apoptotic stage cannot be related to more or less toxicity. According to the available literature [50], different pathways may take from the onset of apoptosis to the stage of complete cell death. Furthermore, the uptake and clearance of apoptotic cells by macrophages may be more complex than a simple removal of cell debris. Hoeppner et al. [51] have demonstrated that blocking engulfment genes in C. elegans embryos improves the cell survival when cells are subjected to weak pro-apoptotic signals. In our study, while EU_2POMo has less cytotoxicity effect almost in the range of other POMs, it interestingly has better cell entry and apoptosis value. A more accurate assessment of the anticancer effects of EU_2POMo appears to be necessary.

4. Conclusion

Achieving new cytotoxic agents with improved effects compared to previous generations has always been the focus of chemists in the field of medicine. Polyoxometalates are considered as the next generation of inorganic anticancer drugs. So designing and synthesis of hybrid conjugates of these compounds using organic molecules that have special properties can be a promis-

ing path for further development. In this study, a new generation of polyoxomolybdate hybrid conjugate was evaluated. Eudesmic acid organo-conjugate of Anderson type manganese polyoxomolybdate (EU_2POMo) was synthesized and evaluated for its cytotoxicity in vitro. Preliminary in vitro cytotoxicity results showed that EU_2POMo has comparable cytotoxicity on cancer breast cell lines (MCF-7 & MDA-MB-231) and interestingly lower cell toxicity on HUVEC normal cells. Furthermore, it seems that the EU can facilitate the entry of POMo into the cell and also emerges more apoptosis value in POMo.

Our preliminary findings from this study convinced us to continue the in vitro and in vivo evaluations on this novel POMo organo-conjugate.

Declaration of Competing Interest

The authors declare that they have no conflicts of interest.

CRediT authorship contribution statement

Maryam Ramezani-Aliakbari: Conceptualization, Methodology, Validation, Formal analysis, Investigation, Data curtion, Writing – original draft, Writing – review & editing. **Azim Soltanabadi:** Methodology, Validation, Formal analysis, Investigation, Data curtion, Supervision. **Hojjat Sadeghi-aliabadi:** Methodology, Validation, Investigation, Data curtion, Supervision. **Jaleh Varshosaz:** Validation, Investigation. **Bahram Yadollahi:** Validation, Data curtion. **Farshid Hassanzadeh:** Resources. **Mahboubeh Rostami:** Conceptualization, Methodology, Validation, Formal analysis, Investigation, Resources, Project administration, Funding acquisition, Data curtion, Writing – original draft, Writing – review & editing, Supervision.

Acknowledgments

We acknowledge the financial support of novel drug delivery systems research center at Isfahan University of Medical Sciences, Grant Number: 298023.

Supplementary materials

Supplementary material associated with this article can be found, in the online version, at doi:10.1016/j.molstruc.2021.130612.

References

[1] https://www.who.int/cancer/prevention/diagnosis-screening/breast-cancer/en/, 2018. 2021).
[2] A. Remesh, Toxicities of anticancer drugs and its management, Int. J. Basic. Clin. Pharmacol. 1 (1) (2012) 1–12.
[3] B.A. Chabner, T.G. Roberts, Chemotherapy and the war on cancer, Nat. Rev. Cancer 5 (1) (2005) 65–72.
[4] H.N. Miras, J. Yan, D..L. Long, L. Cronin, Engineering polyoxometalates with emergent properties, Chem. Soc. Rev. 41 (22) (2012) 7403–7430.
[5] D.E. Katsoulis, A survey of applications of polyoxometalates, Chem. Rev. 98 (1) (1998) 359–388.
[6] J.T. Rhule, C.L. Hill, D.A. Judd, R.F. Schinazi, Polyoxometalates in medicine, Chem. Rev. 98 (1) (1998) 327–358.
[7] T. Yamase, H. Fujita, K. Fukushima, Medical chemistry of polyoxometalates. I: potent antitumor activity of polyoxomolybdates on animal transplantable tumors and human cancer xenograft, Inorg. Chim. Acta 151 (1) (1988) 15–18.
[8] A. Bijelic, M. Aureliano, A. Rompel, Polyoxometalates as potential next-generation metallodrugs in the combat against cancer, Angew. Chem. Int. Ed. 58 (10) (2019) 2980–2999.
[9] A. Boulmier, X. Feng, O. Oms, P. Mialane, E. Rivière, C.J. Shin, J. Yao, T. Kubo, T. Furuta, E. Oldfield, Anticancer activity of polyoxometalate-bisphosphonate complexes: synthesis, characterization, in vitro and in vivo results, Inorg. Chem. 56 (13) (2017) 7558–7565.
[10] Y. Liu, S. Tian, S. Liu, E. Wang, In vitro inhibitory effect of polyoxometalates on human tumor cells, Transit. Met. Chem. 30 (1) (2005) 113–117.
[11] T. Yamase, Anti-tumor,-viral, and-bacterial activities of polyoxometalates for realizing an inorganic drug, J. Mater. Chem. 15 (45) (2005) 4773–4782.
[12] Z..M. Zhang, X. Duan, S. Yao, Z. Wang, Z. Lin, Y..G. Li, L..S. Long, E..B. Wang, W. Lin, Cation-mediated optical resolution and anticancer activity of chiral polyoxometalates built from entirely achiral building blocks, Chem. Sci. 7 (7) (2016) 4220–4229.
[13] H. Zhao, L. Tao, F. Zhang, Y. Zhang, Y. Liu, H. Xu, G. Diao, L. Ni, Transition metal substituted sandwich-type polyoxometalates with a strong metal–C (imidazole) bond as anticancer agents, Chem. Commun. 55 (8) (2019) 1096–1099.
[14] N.A.A. Zahrani, R.M. El-Shishtawy, A.M. Asiri, Recent developments of gallic acid derivatives and their hybrids in medicinal chemistry: a review, Eur. J. Med. Chem. (2020) 112609.
[15] K. Upadhyaya, K. Singh, A. Arun, M. Shukla, N. Srivastava, R. Ashraf, A. Sharma, R. Mahar, S.K. Shukla, J. Sarkar, Identification of gallic acid based glycoconjugates as a novel tubulin polymerization inhibitors, Org. Biomol. Chem. 14 (4) (2016) 1338–1358.
[16] A.S. Negi, Y. Gautam, S. Alam, D. Chanda, S. Luqman, J. Sarkar, F. Khan, R. Konwar, Natural antitubulin agents: importance of 3, 4, 5-trimethoxyphenyl fragment, Bioorg. Med. Chem. 23 (3) (2015) 373–389.
[17] V. Ivasiv, C. Albertini, A.E. Gonçalves, M. Rossi, M.L. Bolognesi, Molecular hybridization as a tool for designing multitarget drug candidates for complex diseases, Curr. Top. Med. Chem. 19 (19) (2019) 1694–1711.
[18] L. Fu, H. Gao, M. Yan, S. Li, X. Li, Z. Dai, S. Liu, Polyoxometalate-based organic–inorganic hybrids as antitumor drugs, Small 11 (24) (2015) 2938–2945.
[19] H..K. Yang, Y..X. Cheng, M..M. Su, Y. Xiao, M..B. Hu, W. Wang, Q. Wang, Polyoxometalate–biomolecule conjugates: a new approach to create hybrid drugs for cancer therapeutics, Bioorg. Med. Chem. Lett. 23 (5) (2013) 1462–1466.
[20] M.S. Hosseini, S.H. Javanmard, L. Rafiei, A.A. Hariri, N. Dana, M. Rostami, Anti-cancer activity of biotin-polyoxomolybdate bioconjugate, EJMO 4 (1) (2020) 42–48.
[21] V.A. Zamolo, G. Modugno, E. Lubian, A. Cazzolaro, F. Mancin, L. Giotta, D. Mastrogiacomo, L. Valli, A. Saccani, S. Krol, Selective targeting of proteins by hybrid polyoxometalates: interaction between a Bis-biotinylated hybrid conjugate and avidin, Front. Chem. 6 (2018) 278.
[22] M.S. Hosseini, S. Haghjooy Javanmard, N. Dana, et al., Novel Tocopherol Succinate-Polyoxomolybdate Bioconjugate as Potential Anti-Cancer Agent, J. Inorg. Organomet. Polym. (2021) 1–13.
[23] D. Ventura, A. Calderan, C. Honisch, S. Krol, S. Serratì, M. Bonchio, M. Carraro, P. Ruzza, Synthesis and biological activity of an A nderson polyoxometalate bis-functionalized with a B ombesin-analog peptide, Pept. Sci. 110 (5) (2018) e24047.
[24] J. Fuchs, I. Brüdgam, Darstellung und eigenschaften des tetrabutylammonium-iso-oktamolybdats [N $(C_4H_9)_4]_4Mo_8O_{26}$/preparation and properties of tetrabutylammonium iso-octamolybdate [N $(C_4H_9)_4]_4Mo_8O_{26}$, Z. Für Naturforschung B 32 (8) (1977) 853–857.
[25] T. Gündüz, N. Gündüz, İ. Şakiyan, A new method for synthesis of manganese (III) acetate dihydrate, Synth. React. Inorg. Met. Org. Chem. 24 (4) (1994) 519–524.
[26] E. Valeur, M. Bradley, Amide bond formation: beyond the myth of coupling reagents, Chem. Soc. Rev. 38 (2) (2009) 606–631.
[27] A.D. Becke, Density-functional thermochemistry. I. The effect of the exchange-only gradient correction, J. Chem. Phys. 96 (3) (1992) 2155–2160.
[28] C. Lee, W. Yang, R.G. Parr, Development of the Colle-Salvetti correlation-energy formula into a functional of the electron density, Phys. Rev. B 37 (2) (1988) 785.
[29] S. Tsuzuki, R. Katoh, M. Mikami, Analysis of interactions between 1-butyl-3-methylimidazolium cation and halide anions (Cl−, Br− and I−) by ab initio calculations: anion size effects on preferential locations of anions, Mol. Phys. 106 (12–13) (2008) 1621–1629.
[30] G. Sun, Y. Chang, S. Li, Q. Li, R. Xu, J. Gu, E. Wang, pH-responsive controlled release of antitumour-active polyoxometalate from mesoporous silica materials, Dalton Trans. (23) (2009) 4481–4487.
[31] N. Gao, H. Sun, K. Dong, J. Ren, T. Duan, C. Xu, X. Qu, Transition-metal–substituted polyoxometalate derivatives as functional anti-amyloid agents for alzheimer's disease, Nat. Commun. 5 (1) (2014) 1–9.
[32] D.M. Morgan, Tetrazolium (MTT) assay for cellular viability and activity, in: Polyamine protocols, Springer, 1998, pp. 179–184.
[33] A. Bahuguna, I. Khan, V.K. Bajpai, S.C. Kang, MTT assay to evaluate the cytotoxic potential of a drug, Bang. J. Pharmacol. 12 (2) (2017) 115–118.
[34] R.I. Freshney, Culture of specific cell types, culture of animal cells: a manual of basic technique, chapter 23 (2005) 375–420.
[35] L.C. Crowley, B.J. Marfell, A.P. Scott, N.J. Waterhouse, Quantitation of apoptosis and necrosis by annexin V binding, propidium iodide uptake, and flow cytometry, Cold Spring Harbor Protoc. 2016 (11) (2016) pdb. prot087288.
[36] G. Geisberger, E.B. Gyenge, D. Hinger, P. Bösiger, C. Maake, G.R. Patzke, Synthesis, characterization and bioimaging of fluorescent labeled polyoxometalates, Dalton Trans. 42 (27) (2013) 9914–9920.
[37] A. Blazevic, A. Rompel, The Anderson–Evans polyoxometalate: from inorganic building blocks via hybrid organic–inorganic structures to tomorrows "Bio-POM, Coord. Chem. Rev. 307 (2016) 42–64.
[38] M.S. Hosseini, L. Rafiei, A. Hariri, N. Dana, M. Rostami, Anticancer activity of biotin polyoxomolybdate bioconjugate, EJMO 4 (1) (2020) 42–48.
[39] P.R. Marcoux, B. Hasenknopf, J. Vaissermann, P. Gouzerh, Developing remote metal binding sites in heteropolymolybdates, Eur. J. Inorg. Chem. 2003 (13) (2003) 2406–2412.
[40] N. Liang, S. Sun, X. Li, H. Piao, H. Piao, F. Cui, L. Fang, α-Tocopherol succinate-modified chitosan as a micellar delivery system for paclitaxel: prepara-

tion, characterization and in vitro/in vivo evaluations, Int. J. Pharm. 423 (2) (2012) 480–488.
[41] S. Schönweiz, M. Heiland, M. Anjass, T. Jacob, S. Rau, C. Streb, Experimental and theoretical investigation of the light-driven hydrogen evolution by polyoxometalate–photosensitizer dyads, Chem. A Eur. J. 23 (61) (2017) 15370–15376.
[42] S. Armaković, S.J. Armaković, M. Vraneš, A. Tot, S. Gadžurić, Determination of reactive properties of 1-butyl-3-methylimidazolium taurate ionic liquid employing DFT calculations, J. Mol. Liq. 222 (2016) 796–803.
[43] V. Jančovičová, M. Čeppan, B. Havlínová, M. Reháková, Z. Jakubíková, Interactions in iron gall inks, Chem. Pap. 61 (5) (2007) 391–397.
[44] J. Zhang, Y. Long, W. Xuan, C. Lin, Y. Song, Preparation of polyoxometalate-chalcone hybrid and its photo-polymerization property, Chin. Sci. Bull. 62 (7) (2017) 685–692.
[45] K.P. Sullivan, W.A. Neiwert, H. Zeng, A.K. Mehta, Q. Yin, D.A. Hillesheim, S. Vivek, P. Yin, D.L. Collins-Wildman, E.R. Weeks, Polyoxometalate-based gelating networks for entrapment and catalytic decontamination, Chem. Commun. 53 (83) (2017) 11480–11483.
[46] Y. Li, M. Liu, L. Chen, Polyoxometalate built-in conjugated microporous polymers for visible-light heterogeneous photocatalysis, J. Mater. Chem. A 5 (26) (2017) 13757–13762.
[47] K.L. Damm, H.A. Carlson, Gaussian-weighted RMSD superposition of proteins: a structural comparison for flexible proteins and predicted protein structures, Biophys. J. 90 (12) (2006) 4558–4573.
[48] A. Blazevic, E. Al-Sayed, A. Roller, G. Giester, A. Rompel, Tris-functionalized hybrid anderson polyoxometalates: synthesis, characterization, hydrolytic stability and inversion of protein surface charge, Chem. A Eur. J. 21 (12) (2015) 4762–4771.
[49] N.I. Gumerova, A. Rompel, Polyoxometalates in solution: speciation under spotlight, Chem. Soc. Rev. (2020).
[50] S. Elmore, Apoptosis: a review of programmed cell death, Toxicol. Pathol. 35 (4) (2007) 495–516.
[51] D.J. Hoeppner, M.O. Hengartner, R. Schnabel, Engulfment genes cooperate with ced-3 to promote cell death in Caenorhabditis elegans, Nature 412 (6843) (2001) 202–206.